Catalysis Today 420 (2023) 114081

Contents lists available at ScienceDirect

Catalysis Today

journal homepage: www.elsevier.com/locate/cattod

Rapid microwave heating and fast quenching for the highly efficient production of long-term stable supported Ag nanoclusters

R. Manno [a,1], P. Ranjan [b,1], V. Sebastian [a,c,d,*], R. Mallada [a,c,d], S. Irusta [a,c,d], E.V. Van der Eycken [b,e], J. Santamaria [a,c,d]

[a] Instituto de Nanociencia y Materiales de Aragón (INMA), CSIC-Universidad de Zaragoza, Zaragoza 50009, Spain
[b] Laboratory for Organic & Microwave-Assisted Chemistry (LOMAC), Department of Chemistry, University of Leuven (KU Leuven), Celestijnenlaan 200F, B-3001 Leuven, Belgium
[c] Networking Research Center CIBER-BBN, 28029 Madrid, Spain
[d] Department of Chemical Engineering and Environmental Technologies, University de Zaragoza, 50018 Zaragoza, Spain
[e] Peoples' Friendship University of Russia (RUDN University), 6 Miklukho-Maklaya Street, 117198 Moscow, Russia

ARTICLE INFO

Keywords:
Nanoclusters
Microwave heating
Ag clusters
Grafting
Catalysis
Alkyne Cyclization

ABSTRACT

Given the exciting potential of metallic clusters in a variety of fields, the development of novel preparation methods to accurately controlling the cluster size has become a research priority. Specifically, for catalytic applications, the synthesis and deployment of metallic nanoclusters on a proper substrate is perhaps the main bottleneck. Here, we have adopted an alternative reactor that uses simultaneous ice cooling and microwave heating (unlike water ice is a low microwave absorber) for the synthesis of Ag nanoclusters directly over a support with ordered mesopores (SBA-15). The reactor design exploits the selectivity of microwave heating, assuring a rapid localized nucleation followed by a nearly instantaneous quenching that largely avoids the aggregation of nascent clusters as well as Ostwald ripening mechanisms. We have compared this new synthesis approach with some previously reported methods for the production of supported silver nanoclusters: conventional batch reactor and also a continuous flow microreactor. The resulting Ag clusters were initially analyzed in terms of size distribution, textural properties and catalytic activity in the reduction of 4-nitrophenol. Finally, encouraged by the good results obtained, these nanoclusters were also employed in the production of different cyclic organic compounds, building blocks for pharmaceutical and photochemical applications. The nanoclusters displayed a high catalytic activity, lowering the metal loading required to achieve high yield and selectivity. Furthermore, the stabilization of the clusters over the mesoporous substrate allowed their reuse in several reaction cycles. In fact, the method produced exceptionally stable Ag clusters, whose catalytic properties were preserved even after one year of storage.

1. Introduction

The catalyst activity directly correlates with the accessibility and the number of available active sites. In homogeneous catalysis, direct contact is assured between reactants and metallic atoms, often resulting in high synthesis yield and selectivity. Even so, catalyst recovery is still a critical factor, negatively impacting economic and environmental aspects. The advances in nanostructured materials have opened numerous opportunities for catalyst design, allowing tuning their structure for the specific application requirements. In heterogeneous catalysis on the other hand, accessibility often becomes an issue and a significant proportion of the metallic phase may not be available for reaction. Catalytic nanoparticles (NPs) are usually supported, to facilitate separation and increase their long-time stability. Ideally, ultrasmall catalytic NPs are desired, to maximize catalyst activity that depends on the available surface area of the NPs [1]. However, depositing well dispersed ultrasmall NPs is challenging, and their stability is often compromised, especially if they are synthesized separately and then supported.

Nanoclusters (NCs) have been heralded as a compromise between unrecoverable single atoms and lower-efficiency NPs. As the particle diameter decreases from 100 to 1 nm, the surface area per unit volume of

* Corresponding author at: Instituto de Nanociencia y Materiales de Aragón (INMA), CSIC-Universidad de Zaragoza, Zaragoza 50009, Spain.
E-mail address: victorse@unizar.es (V. Sebastian).
[1] These authors contributed equally.

https://doi.org/10.1016/j.cattod.2023.114081
Received 6 December 2022; Received in revised form 14 February 2023; Accepted 3 March 2023
Available online 6 March 2023

NPs becomes 100 times higher, increasing the accessibility to the active sites [2]. Furthermore, metal NCs may be stabilized over a proper substrate allowing their application for heterogeneous catalysis. So far, the main routes adopted for the clusters confinement are wet-impregnation and insitu generation. In 2018, Kong et al. [3] and Fan et al. [4] presented two interesting works on glutathione-Au NCs grafted on amino-functionalized silica for fluorescent sensing of heparin and cysteine respectively. The high-density of positive charges in the support represented a powerful tool to attract electrostatically the anionic network of the metallic NCs. Also, impregnating pre-formed particles allows a higher degree of control over the NCs size to be deposited. However, the impregnation method faces important limitations in terms of poor metal loading, no uniform cluster deposition and pore blockage [5,6]. On the other hand, when clusters are generated insitu the yield increases, and obtaining higher metal loadings as well as avoiding pore blockage becomes, in principle, possible. Unfortunately, the majority of the synthesis routes so far reported are characterized by long synthesis time (1–24 h [7–9]) and low control of particle size distribution, with uncontrolled agglomeration [10] and particle growth [11].

Analysis of literature data is sometimes complicated by the fact that the terms “clusters” and “nanoparticles” are often interchangeably used. In this work, we have strived to avoid this confusion by using a strict nomenclature to label either “nanoparticles” or “nanoclusters” using the Kubo criterion and the quantum size effect condition, i.e. for the case of Ag, the threshold diameter is between 1.5 and 2 nm, so particles under this size can properly be called clusters.

We have adapted the simultaneous cooling microwave heating method recently reported by our group to produce Cu clusters [12] for the production of Ag clusters. Thanks to the reactor design used (see below), microwave irradiation was selectively focused on the aqueous solution of silver precursors confined in the porous channels of SBA-15, the only material capable of a strong microwave absorption under the conditions used in the experiment. This material is hydrophilic and significantly adsorbs moisture from the atmosphere [13]. The water inside the pores was immediately heated and the clusters formed. As soon as the microwave power was switched off, a fast cooling ensued, thanks to the simultaneous cooling provided by the ice shell surrounding the reactor (ice is a nearly microwave transparent material at a working frequency of 2.45 GHz [14]). This strategy instantaneously quenched the reaction, and hindered further cluster mobility, resulting in a narrower and more homogeneous NCs distribution.

The physical properties and the catalytic activity of the catalysts prepared were compared in conventional batch reactor [15] and continuous flow microreactor syntheses [16,17]. The results achieved confirm the advantages of the proposed method, giving not only a higher yield of Ag clusters, but also a smaller and more homogeneous particle size. The supported Ag clusters obtained were active catalysts for homogeneous alkynes cyclization [18–24]. The high activity observed was attributed to the cooperative effects of both, the reduced cluster diameter and the presence of highly active uncoordinated atoms surrounding the metal core structure [25]. Finally, the method produced supported Ag clusters of high stability. The catalyst retained its activity even after one year of storage.

2. Materials and methods

2.1. Single step batch synthesis by simultaneous cooling-microwave heating (SCMWH) synthesis of AgNCs@SBA-15

In the reactor design, the materials used are largely microwave-transparent compared to water, i.e. the loss tangent of water is 314, respectively 174, 160 and 560 times higher than that of Pyrex glass, ice,

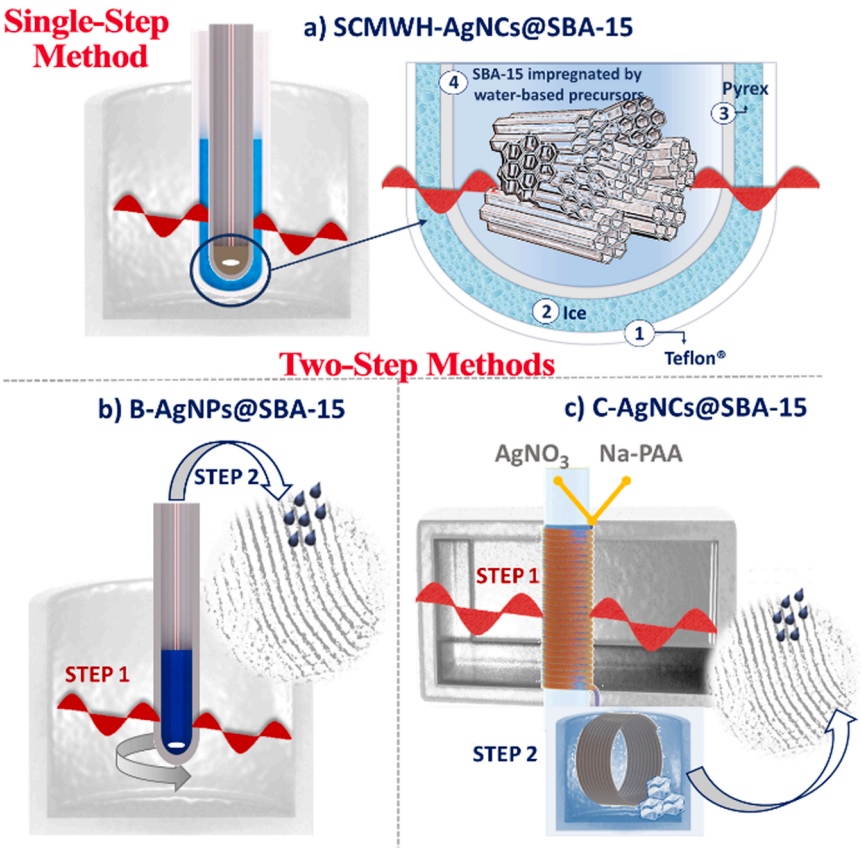

Fig. 1. Single-Step method a) Simultaneous cooling microwave heating reactor set in the commercial CEM Microwave Discover® Cavity and detail of the different zones of the reactor. Two-Step methods. Schematic representation of the batch and continuous flow processes, in b) and c) respectively.

silica and Teflon, meaning that the water present in the ordered support pores will be the main microwave target. As shown in Fig. 1, the simultaneous cooling-microwave heating reactor [12] was formed by two coaxial cylinders, an external Teflon® tube (O.D. 24.5 mm, I.D. 20.7 mm) and an inner coaxial cylinder made of Pyrex (O.D. 16.4 mm, I. D. 13.3 mm), indicated by numbers 1 and 3 in Fig. 1a. The annular space between them was occupied by ice (number 2 in Fig. 1a). The system was precisely fixed in the centre of the open vessel CEM Microwave Discover® Cavity immediately before irradiation, and a thermographic camera (Optris PI-400038T900) recorded the temperature profile on the top surface. The emissivity of each material was considered for the temperature evaluation (ε_{Teflon}=0.85, ε_{Ice}=0.98, ε_{Pyrex}=0.92 and ε_{SBA}=0.79).

100 mg of amino-functionalized SBA-15 [16] was located in the central volume of the inner tube (number 4 in Fig. 1a) after impregnation with 400 μL of fresh precursors' mixture (50 mM of $AgNO_3$ (Aldrich 99.9999%) and 20 μL of poly (acrylic acid, sodium salt) solution (Na-PAA Sigma Aldrich MW 1200, 45 wt% in water), and vigorous stirring for 30 s to assure a homogeneous impregnation. Then, the sample was MW irradiated for 17 s, the water-based precursors inside the ordered pores of SBA-15 were selectively heated, producing the insitu activation of the nucleation-growth mechanism (Fig. 1a). The working power was set at 20 W and the heating was performed at constant power mode. The short duration of the synthesis process ensured that defrosting was minimal, maintaining the low microwave absorption of ice.

As soon as the MW power was switched-off, the reactor was quickly cooled by the surrounding ice, generating a quenching effect. After synthesis, the catalyst was washed by centrifugation at 12,000 rpm for 20 min with distilled water and finally dried at 50 °C overnight. The sample was covered with aluminium foil and stored at 4 °C for 12 months. The sample was identified as SCMWH-AgNCs@SBA-15, where SCMWH stayed for Simultaneous Cooling-Microwave Heating.

2.2. Two-step microwave-assisted synthesis in batch (B) and continuous microfluidic (C) reactors

For the two-step synthesis of catalysts the clusters were first synthesized and stabilized, then in a second step, deposited on the SBA-15 support. In the synthesis by the batch method (catalyst B-AgNPs@SBA-15), we used a procedure previously reported by our group[15]. Briefly, a quartz reactor (I.D. 20.8 mm, O.D. 24.0 mm) was placed in the centre of the open vessel CEM Microwave Discover® Cavity (Fig. 1b). Firstly, 500 μL of Na-PAA was pre-mixed to 10 mL of a 50 mM solution of $AgNO_3$ to obtain a homogeneous starting solution. Then, microwave irradiation was supplied at 200 W for 17 s under high stirring condition (magnetic stirrer bar of Ø4 mm×10 mm). After this MW heating period the reaction mixture was allowed to cool down naturally.

The catalyst synthesis by continuous microfluidic approach (catalyst C-AgNPs@SBA-15) was synthesized in a Microwave-heated continuous flow reactor, previously reported by our group [16] (Fig. 1c). The reactor, made by polytetrafluoroethylene (Teflon®, Iberfluid Instruments, 1/16"x0.04), consisted of three different zones for mixing, heating and, quenching. $AgNO_3$ (50 mM, Aldrich 99.9999%) and poly (acrylic acid, sodium salt) solution (500 μL of Na-PAA Sigma Aldrich MW 1200, 45 wt% in water, dispersed in 9.5 mL of D.W.) were pumped at a flow rate of 0.146 mL/min by a syringe pump (High precision PHD ULTRA by Harvard Apparatus). After rapid mixing in a commercial Y-mixer (material PEEK, IDEX Corporation, thru-hole of 0.02'' and swept volume of 1.7 μL), the precursors reached the heating zone. A helical tubular reactor was irradiated by MWs in a TE10 monomode microwave cavity, under a constant power of 15 W at a resonant frequency of 2.45 GHz. A Vector Network Analyzer and a three stub tuner (GA1002, Gerling Applied Engineering) were employed to maximize the efficiency of the cavity minimizing reflected intensity, S_{11} parameter [26]. The quenching stage was performed in a coil PTFE tubing ($l_{quenching}$=89 cm, $V_{quenching}$=104 μL) immersed in an ice bath and maintained at a constant range of temperature of 0–4 °C.

In both two-step cases, after synthesis, a theoretical concentration of 2.15 wt% of Ag clusters was drop wise added over the SBA-15 rods, and stirring at 1500 rpm was maintained for 1 h. Finally, the catalyst was centrifuged with D.W. at 12,000 rpm for 20 min to separate the non-grafted Ag-NCs and which was dried overnight at 50 °C.

2.3. Characterization techniques – nanocatalyst

The morphological study and the quantification of metal loading were analyzed to discern between the different procedures here adopted.

For the analysis of particle size and their distribution over the porous substrate, a 10 μL drop of Ag@SBA-15 catalyst dispersed in water was deposited onto a holey carbon TEM grid. After complete evaporation, the sample was analyzed by a high-angle annular dark-field scanning transmission electron microscope (HAADF-STEM) FEI Titan™ (80–300 kV) and elemental analysis was carried out with an EDS detector performing in the scanning mode. Furthermore, nitrogen adsorption analysis at 77 K in a Micrometrics ASAP 2020 was performed to evaluate if the grafting of the NCs could have obstructed the SBA-15 pores. The sample was out-gassed at 26.7 Pa and 383 K for 5 h. The Brunauer-Joyner-Halenda (BJH) method was applied to the desorption branch to calculate mean pore diameter (MPD) and pore size distribution. Instead, for the estimation of specific surface area, we applied the Brunauer-Emmett-Teller (BET) method to the adsorption isotherm in the range of relative pressure 0.06–0.19.

For the quantification of the Ag metal loading, we first proceeded with the microwave digestion of 30 mg of the catalyst (200 °C for 20 min in Milestone Ethos Plus microwave cavity) in 5 mL of a mixture of nitric acid (HNO_3) and hydrochloric acid (HCl) in a volume ratio of 1:3. Afterwards, the digested sample was diluted with 25 mL of Milli-Q water, then centrifuged at 12,000 rpm for 20 min and filtered through a hydrophilic syringe filter of 0.2 μm. The transparent solution was finally analyzed by Microwave Plasma Atomic Emission Spectroscopy (MP-AES) (Agilent 4100 MP-AES).

To conclude, X-ray photoelectron spectroscopy (XPS, Axis Supra spectrometer - Kratos Tech), was used to investigate any alterations of the oxidation state of the metallic silver NCs. The samples were excited by a monochromatic AlKα source at 1486.6 eV, run at 12 kV and 10 mA. A survey spectrum was measured at 160 eV pass energy and, for the individual peak regions, spectra were recorded with a pass energy of 20 eV. The peaks were studied by CasaXPS software, adopting a weighted sum of Lorentzian and Gaussian component curves after Shirley background subtraction. The binding energies were referenced to the internal $C_{1\,s}$ standard at 284.9 eV.

2.4. Catalytic activity: 4-nitrophenol reduction

Reduction of 4-nitrophenol by an excess of $NaBH_4$ in water was selected to test the catalytic activity of PAA-Ag NCs supported on SBA-15. In a typical reaction, 1.44 mmol of $NaBH_4$ was added into 30 mL of a fresh solution of 4-nitrophenol (0.125 mM). After collecting the UV-Vis spectrum as a reference of time zero, 1 mg/L of the Ag catalyst (the amount of Ag@SBA-15 was adjusted in each case, based on metal loading) was added keeping the reaction under stirring covered with Aluminium foil. The absorbance peak was analysed every 40 s in a continuous UV-Vis Spectrophotometer (Agilent 8453). For reusability test, the solution was centrifuged after each cycle, observing the deposition of the nanocatalyst as a pellet. The supernatant solution was removed, the residue was dried and then reused with fresh reagents for a different catalytic cycle. To evaluate the possible loss of catalyst during the centrifugation step, we also measured the catalytic activity after 7 consecutive centrifugations without any intermediate reaction.

2.5. Catalytic activity: alkynes cyclization and oxazolidinones synthesis

For 2-(phenylethynyl) phenol cyclization we adopted the same procedure reported in a previous work[16]. For the oxazolidinone synthesis, in an oven-dried 10 mL screw-cap vial propargylic amine (0.12 mmol, 1 equiv), 1,8-diazobicyclo undec-7-ene (DBU) (20 mol%) and Ag NCs (1–0.5 mol%) were suspended in 0.1 M dichloroethane (DCE). The CO_2 was flushed through the reaction mixture using a syringe needle for 2 min. Afterwards, the reaction mixture was placed in a preheated oil bath under CO_2 atmosphere by using a balloon. After 3 h of heating at 50 °C, the mixture was cooled down to room temperature, diluted with ethyl acetate (EtOAc), and filtered through a syringe filter. The solvent was evaporated and the crude product was purified by column chromatography on silica (EtOAc: Heptane = 1: 6–1: 4). The final product was characterized by ^{1}H (400 MHz or 600 MHz) and ^{13}C (100 MHz) NMR (see supporting information for further details).

3. Results and discussion

3.1. Theoretical basis: the borderline between nanoparticles and nanoclusters

Farzin et al. [27]described a NC as a NP with a diameter smaller than 10 nm, for Kauscher et al. [28] the threshold diameter for Au-NCs was 3 nm while for the majority of authors the NCs present a size smaller than 2 nm[2,29,30]. Although there is not a standardized classification, it is commonly recognized that for an ultrasmall size, the electronic energy levels become discrete, generating quantum size effects [30]. Moving from bulk scale to NPs and then to NCs, the number of atoms that form a nanoparticle decreases and, consequently, the spacing between the electronic states becomes progressively higher, resulting in a discretization of the electronic energy states. Considering the Kubo criterion[31] and the quantum size effect condition [32], it is possible to predict the threshold number of atoms and the threshold diameter to discern between NPs and NCs (Eq. 1).

$$\left\{ \begin{array}{l} N < \dfrac{E_F}{K_B T} \\ r > \sqrt[3]{\dfrac{3E_F}{4\pi\rho K_B T}} \end{array} \right\} \quad (1)$$

As reported in Fig. 2, the separation between NCs and NPs is not a fixed value, as it is affected by the number of atoms per unit volume (ρ), the atomic electron configuration, the cluster melting temperature and the temperature of the system[33]. The threshold diameter for the nanocluster-nanoparticle transition ranges between 1.5 and 2 nm for a wide range of metals commonly employed (Ag, Au, Pd, Pt, Cu, and Fe). Then, a NC may be defined as a nano-object with all three external dimensions smaller than 1.5–2 nm, which presents quantum size effects. As reported by Tsukuda et al. [34], we can adopt the term *ultrasmall NCs* when the number of atoms is smaller than 100. In this case, every atom may strongly affect the material properties in a non-scalable regime[2]. When the number of atoms ranges between 100 and 500, the size confinement is less rigorous and the nanostructures, classified as *large-clusters*, progressively recover the metallic behaviour characteristic of a nanoparticle regime, such as conductivity and surface plasmon resonance[35].

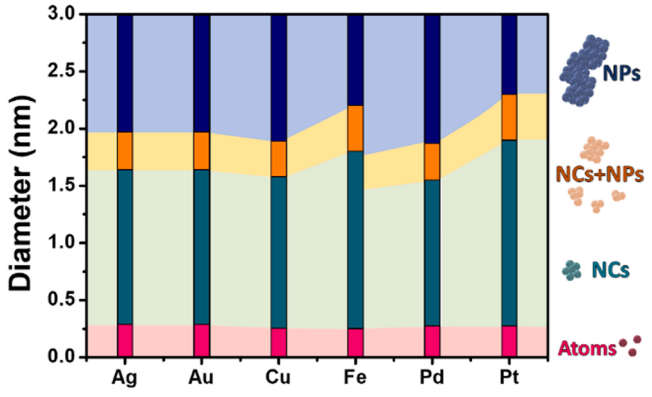

Fig. 2. Schematic representation of threshold diameters to distinguish between single atoms, NCs and NPs for different metals (Ag, Au, Cu, Fe, Pd and Pt). The yellow area corresponds to an overlapping zone where NCs and NPs may coexist. For the calculation, we considered a maximum temperature of 473 K and physical properties of each metal as reported in the literature[32,36,37].

3.2. Nanocatalysts characterization

A nearly instantaneous heating leading to fast nucleation followed by rapid quenching of the reaction are considered crucial aspects for NC production[38,39]. The IR top view thermograms for the simultaneous cooling-microwave heating, reported in Fig. 3, evidenced the desired fast temperature evolution, as well as the selectivity of the heating mechanism afforded by microwaves. Before MW irradiation, the entire reactor was uniformly cooled. When the MW reactor was switched-on, the microwave power was selectively absorbed in the central zone of the reactor, as confirmed by the rapid increase of the temperature reported in the thermal mapping (Fig. 3b, t = 15 s). On the other hand, the surrounding ice remained frozen, drawing heat from the reactor and cooling the system in less than 40 s (Fig. 3b, t = 60 s).

Comparing the nanomaterials prepared with batch [15] and continuous[16] methods (See Fig. S1), the differences in the heating/cooling patterns were reflected in a variation of the particle size distribution. The nanoentities produced with any of the considered approaches have a particle size less than the threshold diameter calculated in Fig. 1 for Ag NPs (1.6–2 nm), therefore can be properly considered as clusters. Clusters produced by the two-step process in the conventional batch reactor B-AgNCs@SBA-15 presented an average size of (1.5 ± 0.4) nm. As reported in Fig. 4a), d) and g), few particles of bigger dimensions were observed, representing less than 2% of the total particles. The distribution further improved with the fast temperature changes afforded by the continuous flow reactor, halving the relative size deviation (1.4 ± 0.2 nm) thanks to the higher control of the heating and quenching steps[16] (Fig. 4b, e and h). In this case, the average temperature during the overall residence time was (71.7 ± 8.7) °C (Fig. S1), a high value that promoted the clusters growth with a final diameter (1.4 ± 0.2 nm) similar to the one achieved by the conventional batch procedure (1.5 ± 0.4 nm), although with less size dispersion. However the best results were obtained with the single-step simultaneous cooling microwave heating protocol. This process allowed to obtain in a single stage (insitu process) a strict control of the particle size distribution with a final size of (1.1 ± 0.3 nm) (Fig. 4c, f and i), 27% lower than in the batch and continuous modes, while the metal load was almost doubled (Table 1). The speed and selectivity of microwave heating were crucial to activate the NC nucleation/reduction and the fast cooling allowing to avoid undesired NC evolution. This is in contrast with the lower metal loading and bigger agglomerates that were observed when the reagents were mixed without microwave irradiation, keeping the impregnated mesoporous support at 12 °C and 4 °C respectively for 60 s and 30 min (Fig. S2.). These results confirm that MW irradiation is highly effective to achieve a fast heating of reagents, an essential feature since temperature control is a key variable on NCs production.

Regarding the metal loading in the SBA-15 mesopores, while the theoretical metal loading (2.15 wt%) was the same for all the procedures studied in this work, but the catalyst SCMWH method allowed to roughly double load of Ag compared to the two-step batch and continuous processes, as confirmed by MP-AES quantification in Error! Reference source not found., giving loading metal yields higher than 80% (compared to less than 50% in two-step methods), without

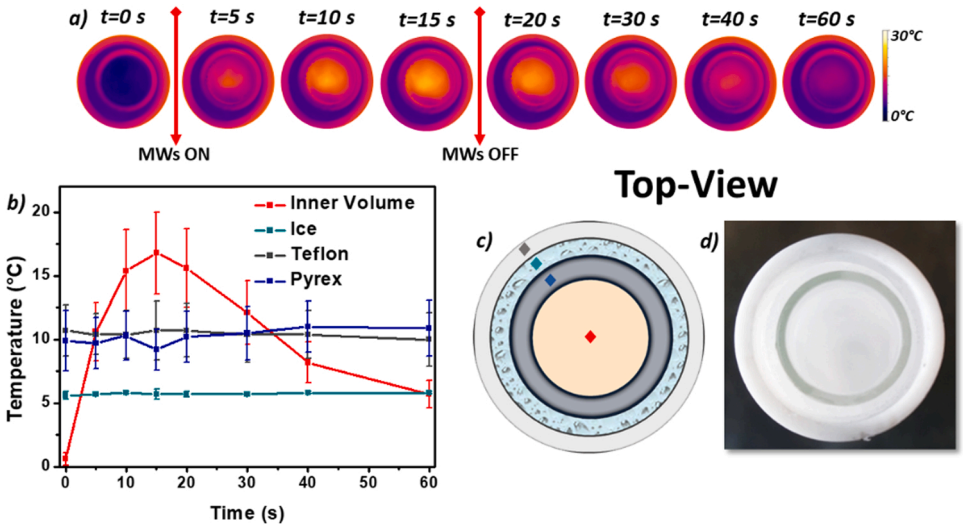

Fig. 3. a) IR thermographs of the top surface of the reactor during the simultaneous cooling-microwave heating synthesis. b) temperature profile of different reactor zones; c) Schematic representation of the reactor zones marked as inner volume (red symbol), pyrex (blue symbol), ice (in green), and Teflon® (in grey) corresponding to the colored temperature curves of Fig. 3b and; d) top view of the reactor.

undesired particle growth. The strong increase of the density of the anchored clusters could be observed in the HAADF-STEM images (Fig. 4) facilitating the contact between the active sites and the molecules of interest during catalysis in the wide SBA-15 pores[40]. However, a critical balance exists between high metal loading and the quality of the sub-nanometer NCs[41]. From economic and environmental points of view, the SCMWH method presents clear advantages, as the loss of high expensive silver precursors and the required amount of SBA-15 support were both reduced compared to other synthesis protocols. Similar results in the same loading range (1–2 wt%), were obtained by more complex and expensive techniques, such as chemical vapour deposition [42], H_2 cold plasma[43] or laser pyrolysis[44].

The textural properties obtained from the analysis of nitrogen adsorption isotherms are presented in Table 1 and Fig. 5. Interestingly, for the catalyst B-AgNCs@SBA-15, the average pore diameter was reduced by 8% (Fig. 5a and Table 1), suggesting that bigger Ag agglomerates may partially reduce the pore accessibility, although this could not be observed with microscopy analysis (Fig. 4a and d). On the contrary, for the two-step continuous C-AgNCs@SBA-15 and single-step SCMWH-AgNCs@SBA-15 samples, the pore diameter was essentially unchanged (9.2 nm, Table 1). This, especially in the case of the SCMWH sample, increases metal loading while avoiding pore obstruction leading to a catalyst with a high concentration of active sites and high accessibility.

Finally, we also studied the effect of the synthesis procedure on the oxidation state of the catalyst, as reported in Fig. 5 and Table 1. The XPS analysis confirmed that the small Ag NCs presented an inner Ag(0) core surrounded by uncoordinated Ag(I) ions stabilized by electrostatic interactions with the PAA network, without relevant variations between them. Clusters are prone to evolve towards larger aggregates during ageing. This modifies the active sites distribution and catalytic activity [45], and usually leads to a decrease of catalytic activity.

In this work, an ageing study was performed on the catalyst SCMWH-AgNCs@SBA-15. This catalyst presented a high concentration of sub-1.5 nm clusters, homogeneously dispersed throughout the SBA-15 channels, even after 12 months of storage at ambient conditions (Fig. 6). Few agglomerates, less than 11% of the total particles counted (Fig. 6-c), were localized at the outer surface of the mesoporous material and presented a diameter higher than 10 nm due to slow and uncontrolled Ostwald ripening mechanism. The agglomeration mechanisms were particularly reported in one of our previous work on unsupported sub 2-nm particles, observing that around 50% of particles increased up to (4.7 ± 1.0) nm after 18 months of storage[15]. The high stability observed in this case suggests that the heterogenization in a mesoporous substrate may increase the stability of the nanocatalyst [33] allowing its repeated use.

3.3. Catalytic activity assessment: 4-nitrophenol reduction

As underlined by Maschmeyer et al. [46], the 4-nitrophenol reduction in aqueous solution is widely reported as a relevant reaction in the field of environmental catalysis and is also often used as a reference test reaction to compare different nanocatalysts.

As reported in Scheme 1, 4-nitrophenol first undergoes deprotonation by hydrolysis of the sodium borohydride in aqueous solution, generating the 4-nitrophenolate ion ($4NP^{-1}$) that presents a characteristic absorbance at a wavelength of 400 nm. Only after the addition of the Ag nanocatalyst, the characteristic absorbance peak of 4-nitrophenolate gradually decreased while the peak of 4-aminophenol (294 nm) increased (Fig. 7a) [47]. Ag clusters interact with the borohydride ions, liberating 4 H^+ due to reduction of water to H_2 [48]. Then, the 4-NP^- absorbs on the catalyst surface and reduction R_I occurs, with the production of intermediate 4-hydroxylaminophenol (4-HAP) and a molecule of H_2O (Scheme 1). In a following step, there is a reversible two-electron transfer reaction R_{II} (Scheme 1), with production of 4-AP. Finally, 4-AP is released and the active site is ready to start a new activation.

Table 2 presents a summary of the pseudo-first order normalized kinetic constant reported for several Ag-based catalysts, ranging from silver nanowires to NPs and NCs, together with NCs prepared by different methods in this work. Since the amount of catalyst has a direct effect on the kinetics, the normalized kinetic constant is calculated by the ratio of the rate constant k to the total concentration of the catalyst added[48]. The Ag nanowires insitu generated by Kong et al. [49] presented a very low activity, which may be correlated with the low surface to volume ratio of nanowires if compared with smaller spherical NPs (entries 1–4 of Table 2). The activity strongly improved for small silver NPs with an average diameter of 7 nm, where the normalized kinetic constant increased up to $1.56{\cdot}10^{-3}$ $s^{-1}{\bullet}L{\bullet}mg^{-1}$ (entry 5 of Table 2) [50]. A further increase of the catalytic activity was observed when the particle diameter was smaller than 2.1 nm, observing the same kinetic order of our small NCs (Table 2 entries 10–12) [51]. No relevant differences were observed between catalysts produced by batch and continuous procedures, suggesting that the small variations observed in

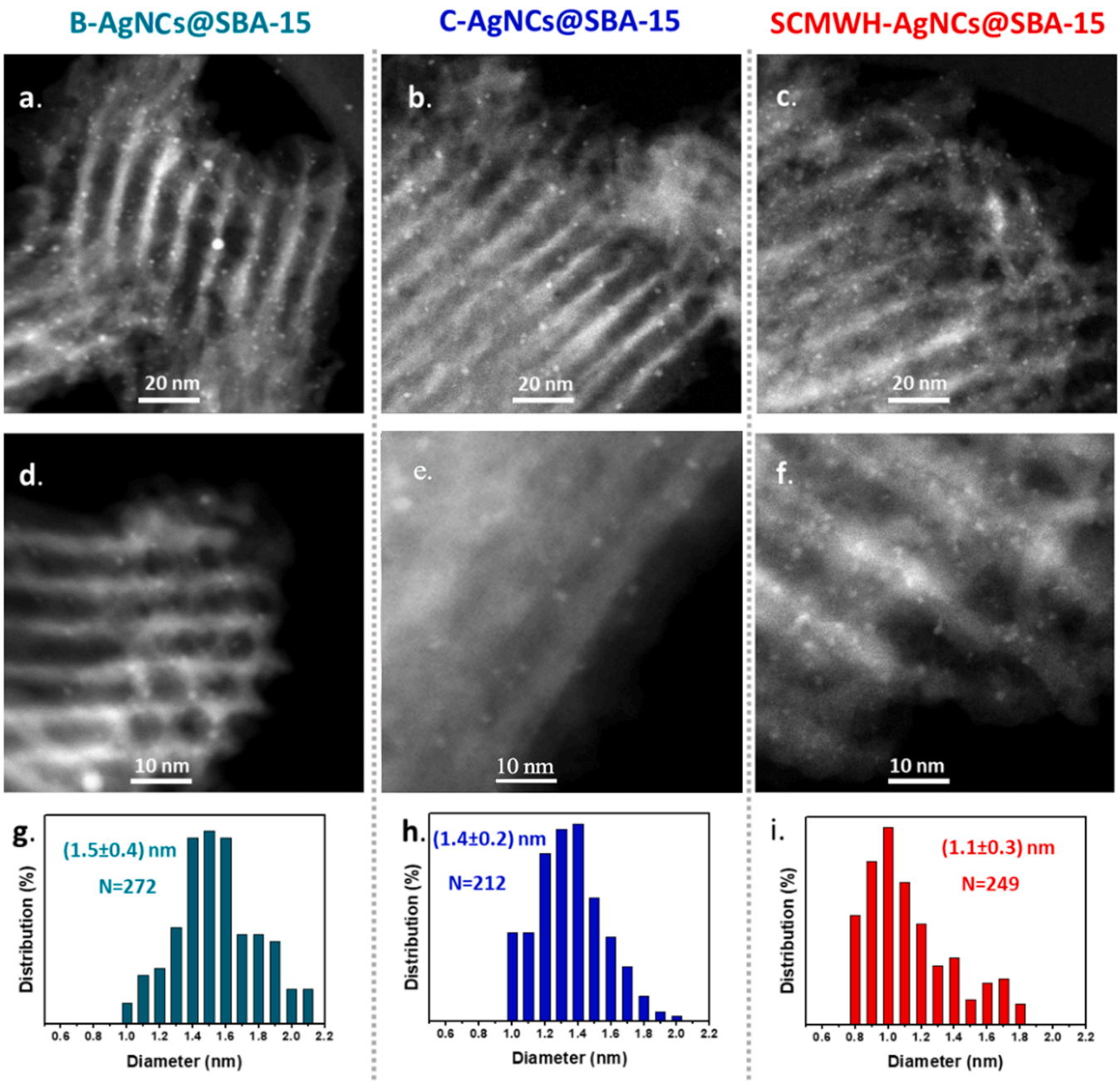

Fig. 4. HAADF-STEM analysis of the three different nanocatalysts, B-AgNCs@SBA-15 (on the left – green color) and C-AgNCs@SBA-15 (in the center– blue color) and SCMWH-AgNCs@SBA-15 (on the right – red color). In figures a, b, and c it is possible to highlight the uniform distribution of silver NPs/NCs along the entire surface of SBA-15 rods. In figures d, e, and f a closer view of the entrance of the pores is presented, without apparent signs of pore obstruction. In figures g, h, and i the relative size distribution of the clusters is presented.

Table 1
Metal loading, synthesis yield, oxidation state and textural properties of the catalyst designed.

Catalyst	Ag Loading wt%	Loading Yield (%)	S_{BET} (m^2g^{-1})	V_t (cm^3g^{-1})	D_{BJH} (nm)	Ag^0	Ag^{+1}
SBA-15	-	-	317	0.89	9.3	-	-
B-AgNPs@SBA-15	0.98 ± 0.05	43–48	266	0.76	8.6	45%	55%
C-AgNCs@SBA-15	0.96 ± 0.07	41–48	255	0.59	9.2	50%	50%
SCMWH-AgNCs@SBA-15	1.80 ± 0.08	80–87	245	0.69	9.2	49%	51%

cluster size and Ag species ratio (Ag0 and AgI) may not be significant enough to affect the reaction.

The catalyst SCMWH-AgNCs@SBA-15 with a normaliced kinetic constant of $(15.98 \pm 0.42)10^{-3}$ s^{-1}•L•mg^{-1} was more than two times more active in comparison with B-AgNCs@SBA-15 and C-AgNCs@SBA-15. The density of anchored clusters represented a critical aspect. As

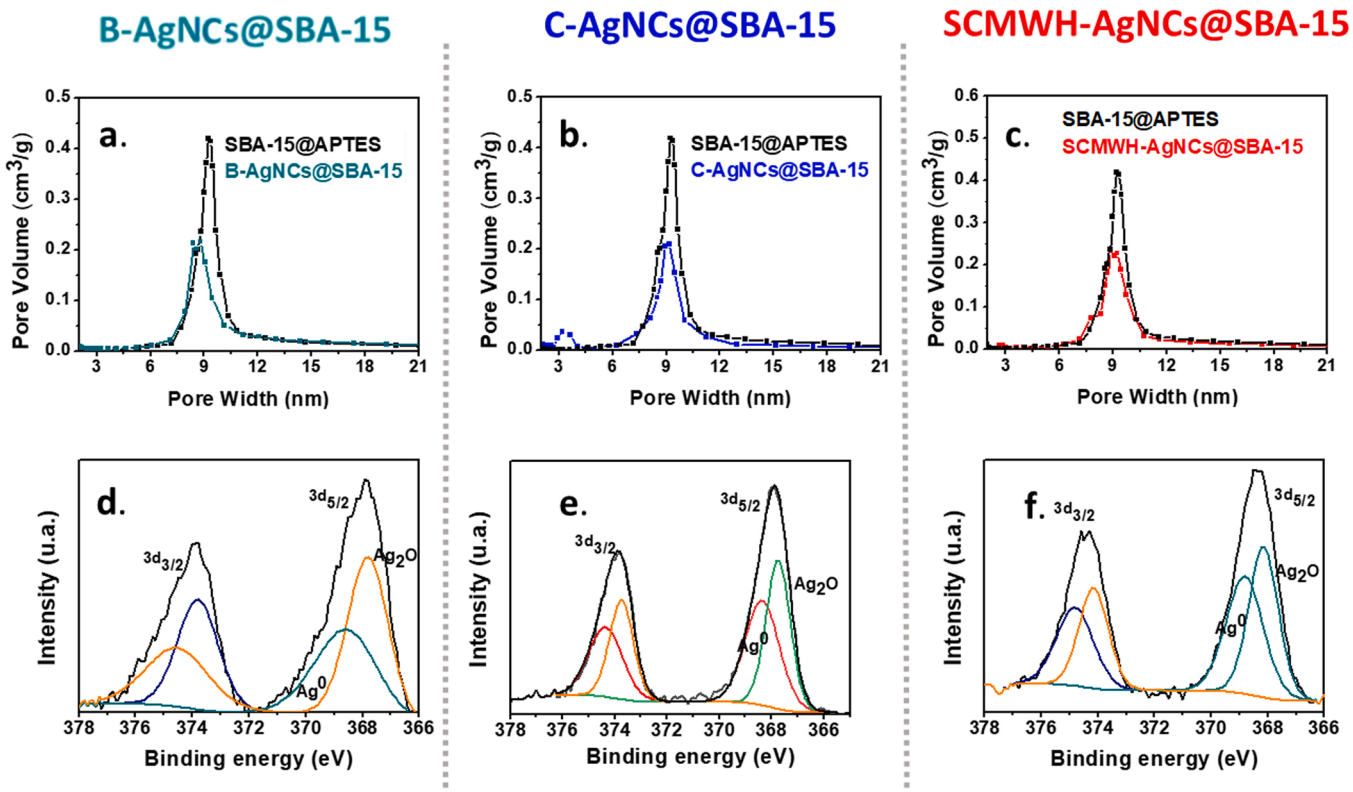

Fig. 5. N_2-adsorption and XPS analysis for B-AgNCs@SBA-15 (a and d), C-AgNCs@SBA-15 (b and e) and SCMWH-AgNCs@SBA-15 (c and f).

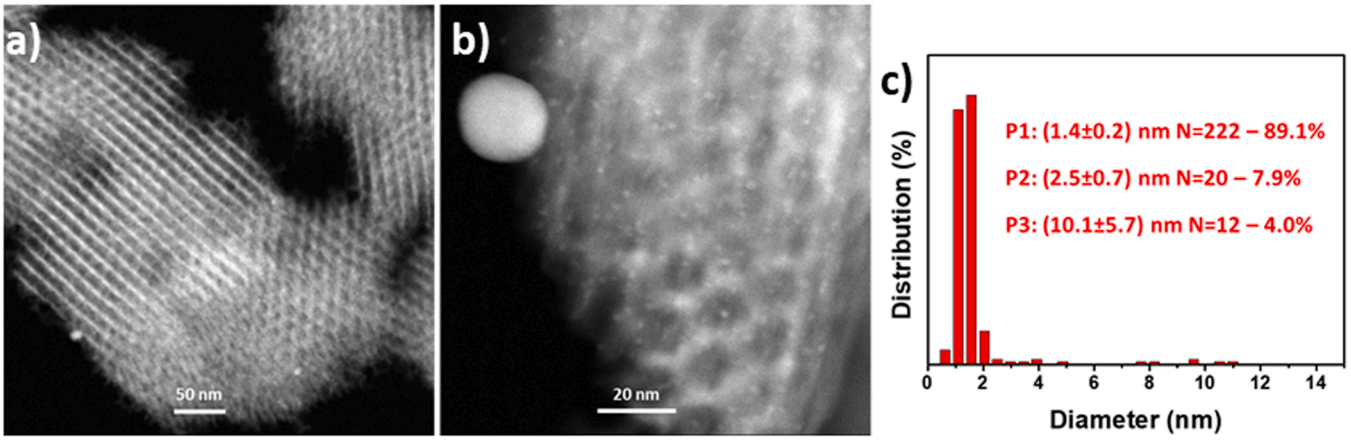

Fig. 6. a) and b) HRSTEM and c) size distribution of catalyst SCMWH-AgNCs@SBA-15 after one year of storage at ambient conditions.

confirmed by Lin et al. [51], the higher the loading density, the higher the probability of contact between the 4-nitrophenolate, hydrogen and the metallic surface. The catalyst SCMWH-AgNCs@SBA-15 (metal loading 1.8 wt%) presented a normalized kinetic value close to the entries 7 and 8 of Table 2, obtained with 2.1 nm-AgNPs and a metal loading of 2.6–3.0 wt%. The higher activity of SCMWH-AgNCs@SBA-15 compared to B-AgNCs@SBA-15 and C-AgNCs@SBA-15 may be explained by the faster adsorption/desorption on closest Ag active sites and the shorter diffusion distance required for 4-nitrophenolate ions to interact with H_2 at the Ag catalytic surface [52].

After 8 cycles of catalysis, the catalyst was separated from the liquid phase by centrifugation, and its activity was measured, as reported in Fig. 7. It can be seen that after 8 cycles the kinetic activity decreased by 43%, 25%, and 17% respectively for SCMWH-AgNCs@SBA-15, B-AgNCs@SBA-15 and C-AgNCs@SBA-15. The apparent drop in the activity seems to be mainly due to the loss of catalyst that takes place during the recovery process using centrifugation, as previously reported also by Cheng *et al.* [53]. The hypothesis was experimentally verified by the evaluation of the catalytic activity of SCMWH-AgCs@SBA-15 after 7 consecutive centrifugations without intermediate 4-nitrophenol reduction reactions in deionized water, reporting a kinetic constant of $10.41 \bullet 10^{-3}$ $s^{-1} \bullet L \bullet mg^{-1}$, 35% lower than the initial value (Fig. 7e in grey). Furthermore, the gradual loss of the catalyst in the cleaning process may explain the higher reduction observed for the catalyst SCMWH-AgNCs@SBA-15 compared to B-AgNCs@SBA-15 and C-AgNCs@SBA-15 catalysts, since the metal loading is the highest (Table 1).

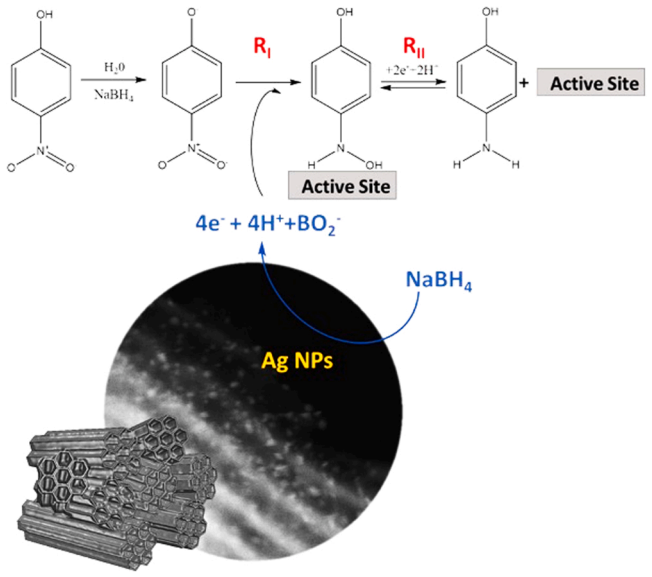

Scheme 1. Reaction mechanism of 4-NP reduction in an excess of $NaBH_4$.

3.4. Catalytic activity: alkyne cyclization

Encouraged by the superior characteristics of the SCMWH catalyst demonstrated using the reduction of 4-NP as a test reaction, we proceeded to use it in an alkyne cyclization, a system where Ag nanostructures can play a role as efficient catalysts. The alkyne functional group represents one of the most versatile building blocks of organic chemistry, due to its unusual and attractive features. The presence of two π-systems in the alkyne functional group allows it to form four new bonds, leading to the atom economical synthesis of complex molecular architectures in a cascade manner [54]. However, the activation of the alkyne moiety is crucial to fully tap into the potential of this fundamental functional group [55]. In this regard, silver catalysts hold an important position towards the activation of alkynes through either π-activation or both π − and σ-activation modes. In the last decades, silver-catalysed transformations have provided a plethora of important compounds in medicinal, agrochemical and material fields [56].

A sustainable methodology should be able to generate various heterocyclic scaffolds by overpassing waste generation and metal contamination. In this work, we have achieved the synthesis of oxazolidinones in a more economical and greener way by employing AgNCs as heterogeneous catalysts. The dual nature of Ag NCs (Ag(0)/Ag(I)) ensured high activity for the cyclization of 2-(phenylethynyl)phenol, in contrast to silver salts or large NPs [16]. Notably, the catalyst SCMWH-AgNCs@SBA-15 showed almost similar efficiency after one year of storage (yield decrease lower than 4%), Fig. 8(t = 450 min). Furthermore, the heterogeneous catalyst SCMWH-AgNCs@SBA-15 was approximately 3.5 times more active than homogeneous catalysts under equivalent conditions, at 50 °C with 1.5 mol.% of Ag. The excellent catalytic efficiency, the reusability and the long-time stability of the catalyst are key-aspects for its potential industrial application.

Since oxazolidinones have a wide application in pharmaceutical science and in enantioselective synthesis, we employed Ag NCs for the synthesis of oxazolidinones in the presence of CO_2 and propargylic amines. The utilization of CO_2 in cycloaddition reactions is an elegant and environmental friendly approach to generate various important scaffolds. As our long-standing goal [57,58] was to steer the synthesis of oxazolidinones in a more economical and greener way, we commenced our investigation with propargylamine **1**, CO_2 and Ag NCs using dichloroethane (DCE) as a solvent. We observed the formation of the desired product **2** with 13% yield (Table 3, entry 1). This type of reactivity was for the first time reported by Yamada and co-workers with Ag salts in 2009[57]. To further improve the yield of the desired product **2**, we added 1,8-diazobicyclo-undec-7-ene (DBU) to facilitate CO_2 fixation under our mild reaction conditions. Indeed, DBU has been reported as an

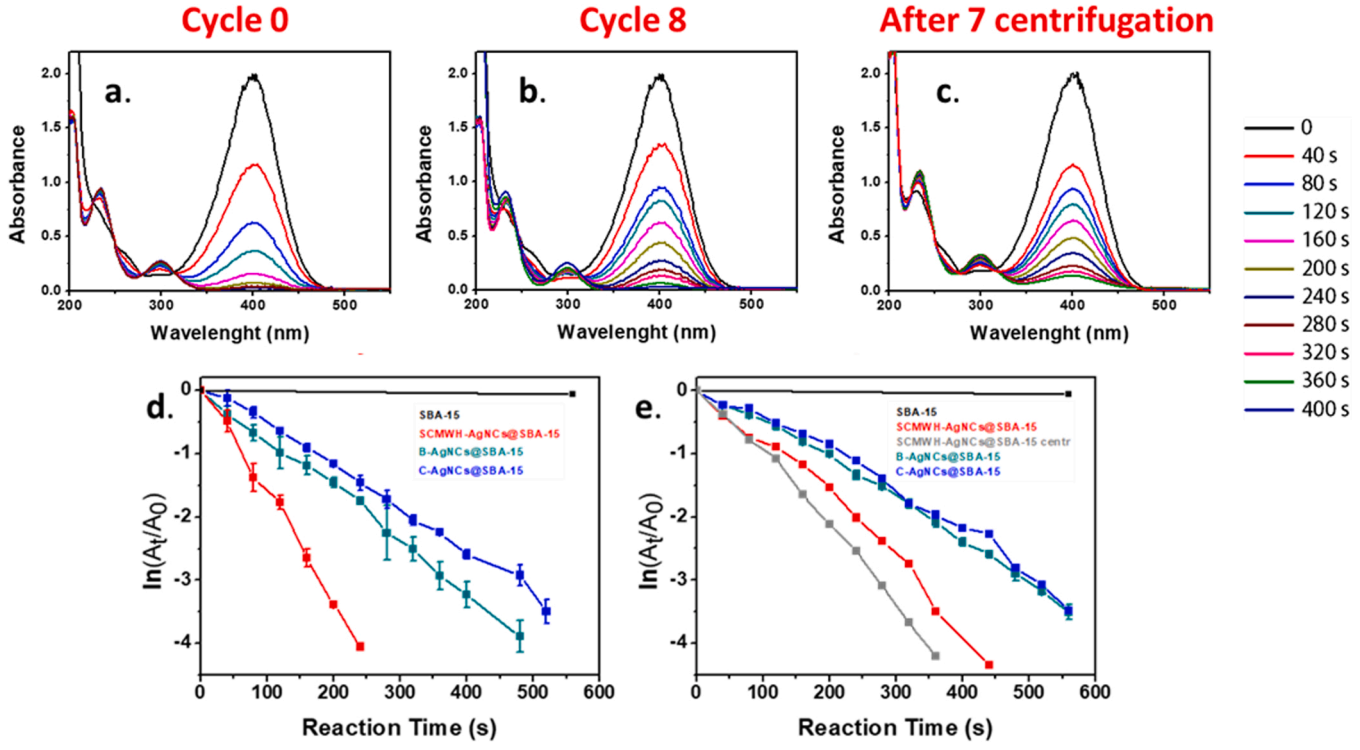

Fig. 7. UV-Vis spectrophotometry 4-nitrophenol reduction study for SCMWH catalyst at cycle 0 (a), cycle 8 (b) and after 7 centrifugations without intermediate 4-nitrophenol reduction reactions in deionized water (c). Kinetic analysis at cycle 0 and cycle 8, d and e respectively. All the measurements were performed with a concentration of 1 mg/L of Ag.

Table 2
A summary of Normalized Kinetic Constant for the reduction of 4-NP catalysed by Ag nanowires, Ag NPs and Ag NCs at different metal loading. The Normalized Kinetic Constant was calculated considering the ration between the rate constant (s^{-1}) and the Ag concentration (mg_{Ag}/L) used as catalyst.

Entry	Sample	Ag Morphology	Ag Loading (wt%)	K (s^{-1}•L•mg^{-1})
1	0.7Ag-SBA-15[49]	Nanowires	9.26	$2.27•10^{-5}$
2	0.5Ag-SBA-15[49]	Nanowires	7.89	$2.17•10^{-5}$
3	0.3Ag-SBA-15[49]	Nanowires	6.52	$1.73•10^{-5}$
4	0.1Ag-SBA-15[49]	Nanowires	5.45	$1.53•10^{-5}$
5	Ag10 @SBA-15[50]	NPs-7 nm	10	$1.56•10^{-3}$
6	MSAg-50[51]	NPs/NCs (< 2.1 nm)	3.5	$33.71•10^{-3}$
7	MSAg-70[51]	NPs/NCs (< 2.1 nm)	3.2	$19.06•10^{-3}$
8	MSAg-90[51]	NPs/NCs (< 2.1 nm)	3	$15.70•10^{-3}$
9	MSAg-110[51]	NPs/NCs (< 2.1 nm)	2.6	$15.38•10^{-3}$
10	*B-AgNCs@SBA-15*	(1.5 ± 0.4) nm	(0.98 ± 0.05)	(7.90 ± 0.58)• 10^{-3}
11	*C-AgNCs@SBA-15*	(1.4 ± 0.2) nm	(0.96 ± 0.07)	(6.70 ± 0.22)• 10^{-3}
12	*SCMWH-AgNCs@SBA-15*	(1.1 ± 0.3) nm	(1.80 ± 0.08)	(15.98 ± 0.42)• 10^{-3}

efficient trapping agent and activator for the thermodynamically and kinetically stable CO_2 molecule [59]. To our delight, the optimized reaction conditions allowed us to obtain product **2** with 94% yield (Table 3, entry 6). This resulted in a 13 h time-reduction if compared with the homogeneous data [60] (92% yield was reported after 16 h with 0.5 mol% of AgO_2). Longer reaction times were required for $AgNO_3$ (95% - 20 h) and AgOAc (90% - 18 h). AgNPs of 20–35 nm supported on covalent organic frameworks (COF) [61] presented a slightly better result with a yield of 95% after 3 h at room temperature, but employing a molar concentration 24 times higher as compared to the Ag NCs employed in this work. In both cases, the supported catalysts allowed easy recovery and reuse. In the case of the highly precious PdNPs of 6 nm stabilized on a porous organic polymer, the reaction time was reduced to 30 min employing 10 mol% of the catalyst ($T_r = 80$ °C) [62]. On the contrary, 12 h were required to obtain 95% yield with COF@Cu NCs (39 mol%) [63], confirming that silver may still cover the gap between the low activity Cu- and highly expensive Pd-based solutions. A plausible mechanism based on our observations and literature reports is shown in Scheme 2. The less or no formation of our desired product in the absence of DBU and Ag NCs showed the necessity of both for this transformation [60].

To prove the generality of our optimized reaction conditions, we examined the reactivity of different *N*-alkyl substituted terminal propargylic amines, delivering the corresponding desired products in good to excellent yields (see Table 4, entries 1–5). Furthermore, the recyclability of the Ag NCs under our optimized conditions showed no decrease in yield even after 4 catalytic cycles (See Fig. S3).

4. Conclusions

The fast and selective heating provided by a microwave field has been exploited for the innovative design of a simultaneous cooling-microwave heating reactor able to produce a Ag NCs catalyst in a

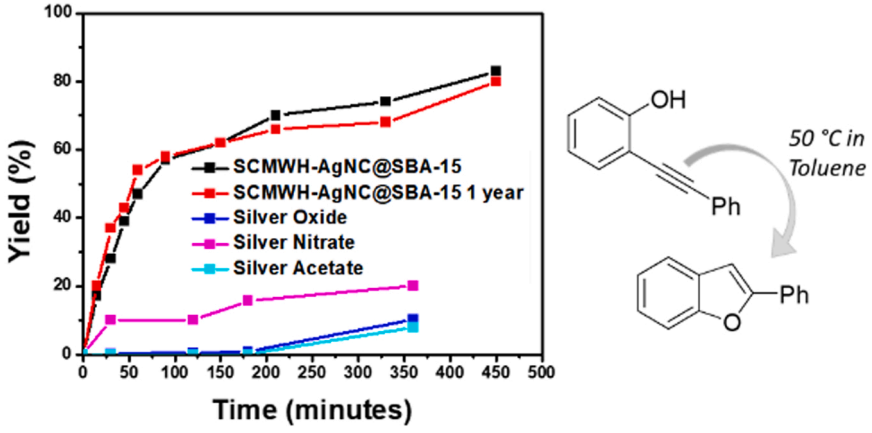

Fig. 8. Test of long-time stability of the catalytic activity of SCMWH-AgNCs@SBA-15 (1.5 molar %) for cyclization of 2-(phenylethynyl)phenol.

Table 3
Optimization of the synthesis of oxazolidinones via CO_2 capture catalysed by SCMWH-AgNCs@SBA-15 with the different concentrations of DBU.

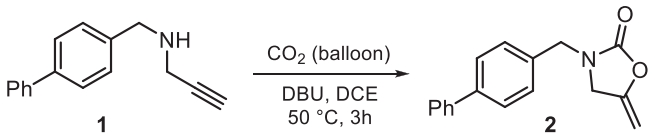

Entry	Mol % Ag	Additive	Temp (°C)	Time (h)	Yield (%)
1	0.5	DBU (0 equiv)	50	3	13
2	-	DBU (1equiv)	50	3	0
3	1	DBU (1equiv)	50	3	94
4	0.5	DBU (1equiv)	50	3	94
5	0.5	DBU (0.5 equiv)	50	3	94
6	0.5	DBU (0.2 equiv)	50	3	94

[a]Reaction conditions: All reactions were run with **1** (0.12 mmol) in DCE (1.2 mL) in a screw cap vial. Yields were determined by the NMR-integration method using 1,3,5-trimethoxybenzaldehyde as an internal standard.

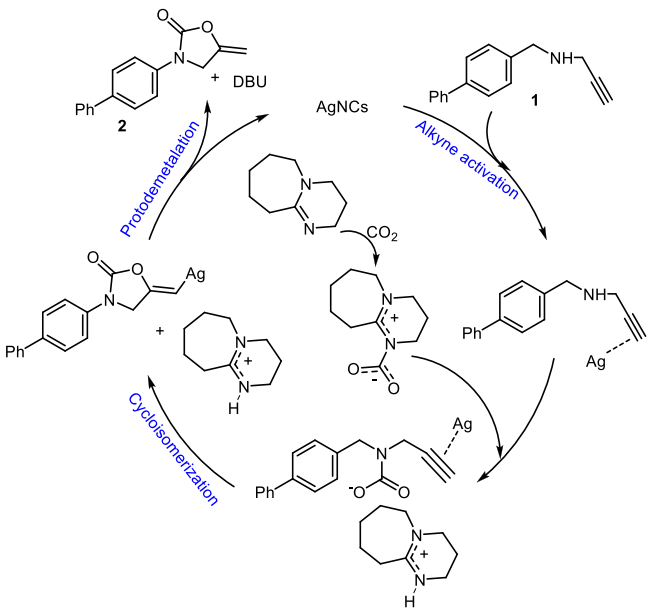

Scheme 2. Reaction mechanism of oxazolidinone synthesis by CO_2 capture. [60,61].

Table 4
Substrate scope for oxazolidinone synthesis.

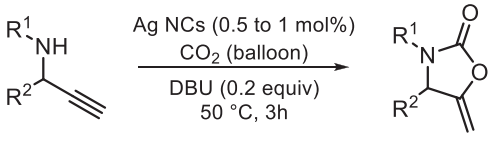

1a 2a

Entry	Product	Time (h)	Temp (°C)	Yield (%)
1	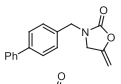	3	50	94
2		3	50	90
3		3	50	80
4	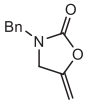	3	50	66
5	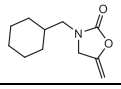	3	50	99

[a]Reaction conditions: All reactions were run with **1a** (0.12 mmol) in DCE (1.2 mL) in a screw cap vial. Yields were determined by the NMR-integration method using 1,3,5-trimethoxybenzaldehyde as an internal standard.

single stage. The insitu nucleation and the fast quenching realized in this new approach was able to generate a homogeneous nucleation throughout the catalyst support and stops cluster growth at an average size of (1.1 ± 0.3) nm, 29% lower than the catalyst produced by the batch and continuous two-step approaches, where the clusters were first generated and then deposited on the support. With the SCMWH approach the clusters were homogeneously distributed throughout the mesoporous silica support, with a high density and without noticeable decrease of pore size. Furthermore, the loading yield increased above 80% without relevant variation of the oxidation state, with the simultaneous presence of Ag(I) and Ag(0).

The reduction of cluster-cluster distance resulted in a faster absorption/desorption on closest Ag active sites and a shorter diffusion distance, as confirmed by 4-nitrophenol reduction tests. The catalytic performance was as good as the best reported in literature but with a lower metal loading. This remarkable performance was rationalized by the faster adsorption/desorption on closer Ag active sites and the shorter diffusion distance required for interacting with reagents. The catalyst was stable even after one year of storage, as confirmed by microscopy and catalytic characterization. Furthermore, an extraordinary catalytic enhancement for both 2-(phenylethynyl)phenol and oxazolidinone synthesis was demonstrated using mild reaction conditions. The higher activity of supported clusters if compared to homogeneous silver salts, together with the possibility of reusing the catalyst for different cycles, highlights the potential of this innovative NCs synthesis method for a breadth of catalytic reactions.

CRediT authorship contribution statement

R. Manno: Data curation, Formal analysis. **P. Ranjan:** Data curation, Formal analysis, Writing – original draft. **V. Sebastian:** Conceptualization, Data curation, Formal analysis, Funding acquisition, Supervision, Validation, Writing – review & editing. **R. Mallada:** Conceptualization, Funding acquisition, Supervision, Validation, Writing – original draft, Writing – review & editing. **S. Irusta**: Data curation, Formal analysis. **E.V. Van der Eycken:** Conceptualization, Funding acquisition, Supervision, Validation, Writing – review & editing. **J. Santamaria:** Conceptualization, Funding acquisition, Supervision, Validation, Writing – review & editing.

Declaration of Competing Interest

The authors declare that they have no known competing financial interests or personal relationships that could have appeared to influence the work reported in this paper.

Data availability

Data will be made available on request.

Acknowledgements

This project has received funding from the European Union's Horizon 2020 research and innovation programme under the Marie Skłodowska-Curie grant agreement no. 721290 (recipient RM and PR; experiments and writing). This publication reflects only the author's view, exempting the Community from any liability. Project website: http://cosmicetn.eu/. V.S. acknowledged the financial support from Ministerio de Ciencia, Innovación y Universidades, Programa Retos Investigación, Proyecto REF: PID2021-127847OB-I00. Financial support from CIBERBBN (initiative funded by the VI National R&D&i Plan 2008 −2011, Iniciativa Ingenio 2010, Consolider Program, CIBER Actions and financed by the Instituto de Salud Carlos III with assistance from the European Regional Development Fund) is gratefully acknowledged (recipient VS,RM,SI, JS: experiments, writing and supervision). This paper has been supported by the RUDN University Strategic Academic Leadership Program (recipient EVdE; writing and supervision). ICTS ELECMI-LMA and NANBIOSIS are gratefully acknowledged.

Appendix A. Supporting information

Supplementary data associated with this article can be found in the online version at doi:10.1016/j.cattod.2023.114081.

References

[1] J.A. Dumesic, G.W. Huber, M. Boudart, Principles of heterogeneous catalysis, in: G. Ertl, H. Knözinger, F. Schüth, J. Weitkamp (Eds.), Handb. Heterog. Catal., KGaA, Wiley-VCH Verlag GmbH& Co., 2007, pp. 1–15.

[2] L. Liu, A. Corma, Metal catalysts for heterogeneous catalysis: from single atoms to nanoclusters and nanoparticles, Chem. Rev. 118 (2018) 4981–5079, https://doi.org/10.1021/acs.chemrev.7b00776.

[3] L. Ma, M. Zhang, A. Yang, Q. Wang, F. Qu, F. Qu, R.M. Kong, Sensitive fluorescence detection of heparin based on self-assembly of mesoporous silica nanoparticle-gold nanoclusters with emission enhancement characteristics, Analyst 143 (2018) 5388–5394, https://doi.org/10.1039/c8an01556b.

[4] N. Xu, Y. Yuan, C. Lan, W. Wei, L. Meng, L. Fan, A novel dual-emission fluorescent nanohybrid containing silica nanoparticles and gold nanoclusters for ratiometric determination of cysteine based on turn-on fluorescence strategy, New J. Chem. 42 (2018) 10092–10099, https://doi.org/10.1039/c8nj01528g.

[5] S. Zhang, S. Muratsugu, N. Ishiguro, M. Tada, Ceria-doped Ni/SBA-16 catalysts for dry reforming of methane, 1885–1864, ACS Catal. 3 (2013), https://doi.org/10.1021/cs400159w.

[6] Y. Soni, I. Kavya, T.G. Ajithkumar, C.P. Vinod, One pot ligand exchange method for a highly stable Au-SBA-15 catalyst and its room temperature CO oxidation, Chem. Commun. 54 (2018) 12412–12415, https://doi.org/10.1039/C8CC06887A.

[7] F. Ulusal, E. Erünal, B. Güzel, Green preparation of Pd nanoparticles on SBA-15 via supercritical fluid deposition and application on Suzuki–Miyaura cross-coupling reaction, J. Nanopart. Res. 20 (2018) 219–232, https://doi.org/10.1007/s11051-018-4325-0.

[8] L.R. Shultz, L. Hu, K. Preradovic, M.J. Beazley, X. Feng, T. Jurca, A broader-scope analysisof the catalytic reduction of nitrophenols and azo dyes with noble metal nanoparticles, ChemCatChem 11 (2019) 2590–2595, https://doi.org/10.1002/cctc.201900260.

[9] Z. Zhang, Y. Luo, Y. Guo, W. Shi, W. Wang, B. Zhang, R. Zhang, X. Bao, S. Wu, F. Cui, Pd and Pt nanoparticles supported on the mesoporous silica molecular sieve SBA-15 with enhanced activity and stability in catalytic bromate reduction, Chem. Eng. J. 344 (2018) 114–123, https://doi.org/10.1016/j.cej.2018.03.056.

[10] Y. Yang, C. Ochoa-Hernández, V.A. De La Peña O'Shea, J.M. Coronado, D. P. Serrano, Ni2P/SBA-15 as a hydrodeoxygenation catalyst with enhanced selectivity for the conversion of methyl oleate into n-octadecane, ACS Catal. 2 (2012) 592–598, https://doi.org/10.1021/cs200659r.

[11] L. Uson, J.L. Hueso, V. Sebastian, R. Arenal, I. Florea, S. Irusta, M. Arruebo, J. Santamaria, In-situ preparation of ultra-small Pt nanoparticles within rod-shaped mesoporous silica particles: 3-D tomography and catalytic oxidation of n-hexane, Catal. Commun. 100 (2017) 93–97, https://doi.org/10.1016/j.catcom.2017.06.022.

[12] L. Song, R. Manno, P. Ranjan, V. Sebastian, S. Irusta, R. Mallada, L. Van Meervelt, J. Santamaria, E.V. Van der Eycken, Preparation of Cu cluster catalysts by simultaneous cooling–microwave heating: application in radical cascade annulation, Nanoscale Adv. (2021).

[13] A. Centineo, H.G.T. Nguyen, L. Espinal, J.C. Horn, S. Brandani, An experimental and modelling study of water vapour adsorption on SBA-15, Microporous Mesoporous Mater. 282 (2019) 53–72, https://doi.org/10.1016/j.micromeso.2019.03.018.

[14] C.O. Kappe, D. Dallinger, S.S. Murphree, Practical Microwave Synthesis for Organic Chemists: Strategies, Instruments, and Protocols, 2008.

[15] R. Manno, V. Sebastian, S. Irusta, R. Mallada, J. Santamaria, Ultra-small silver nanoparticles immobilized in mesoporous SBA-15. Microwave-assisted synthesis and catalytic activity in the 4-nitrophenol reduction, Catal. Today 362 (2021) 81–89, https://doi.org/10.1016/j.cattod.2020.04.018.

[16] R. Manno, P. Ranjan, V. Sebastian, R. Mallada, S. Irusta, U.K. Sharma, E.V. Van der Eycken, J. Santamaria, Continuous microwave-assisted synthesis of silver nanoclusters confined in mesoporous SBA-15: application in alkyne cyclizations, Chem. Mater. 32 (2020) 2874–2883, https://doi.org/10.1021/acs.chemmater.9b04935.

[17] R. Manno, V. Sebastian, R. Mallada, J. Santamaria, 110th anniversary: nucleation of Ag nanoparticles in helical microfluidic reactor. Comparison between microwave and conventional heating, Ind. Eng. Chem. Res. 58 (2020), https://doi.org/10.1021/acs.iecr.9b01460.

[18] G. Fang, X. Bi, Silver-catalysed reactions of alkynes: recent advances, Chem. Soc. Rev. 44 (2015) 8124–8173, https://doi.org/10.1039/c5cs00027k.

[19] E. Parker, N. Leconte, T. Godet, P. Belmont, Silver-catalyzed furoquinolines synthesis: From nitrogen effects to the use of silver imidazolate polymer as a new and robust silver catalyst, Chem. Commun. 47 (2011) 343–345, https://doi.org/10.1039/c0cc02623a.

[20] A. Zuliani, P. Ranjan, R. Luque, E.V. Van der Eycken, Heterogeneously catalyzed synthesis of imidazolones via cycloisomerizations of propargylic ureas using Ag and Au/Al SBA-15 systems, ACS Sustain. Chem. Eng. 7 (2019) 5568–5575, https://doi.org/10.1021/acssuschemeng.9b00198.

[21] P. Ranjan, G.M. Ojeda, U.K. Sharma, E.V. Van der Eycken, Metal-Free dearomatization: direct access to spiroindol(en)ines in batch and continuous-flow, Chem. Eur. J. 25 (2019) 2442–2446, https://doi.org/10.1002/chem.201805945.

[22] X. Bantreil, A. Bourderioux, P. Mateo, C.E. Hagerman, M. Selkti, E. Brachet, P. Belmont, Phosphine-triggered selectivity switch in silver-catalyzed o-alkynylbenzohydroxamic acid cycloisomerizations, Org. Lett. 18 (2016) 4814–4817, https://doi.org/10.1021/acs.orglett.6b02235.

[23] Z. Chang, X. Jing, C. He, X. Liu, C. Duan, Silver clusters as robust nodes and π-activation sites for the construction of heterogeneous catalysts for the cycloaddition of propargylamines, ACS Catal. 8 (2018) 1384–1391, https://doi.org/10.1021/acscatal.7b02844.

[24] D.S. Ermolat'Ev, J.B. Bariwal, H.P.L. Steenackers, S.C.J. De Keersmaecker, E. V. Van der Eycken, Concise and diversity-oriented route toward polysubstituted 2-aminoimidazole alkaloids and their analogues, Angew. Chem. - Int. Ed. 49 (2010) 9465–9468, https://doi.org/10.1002/anie.201004256.

[25] S.G. Sudrik, N.K. Chaki, V.B. Chavan, S.P. Chavan, S.P. Chavan, H.R. Sonawane, K. Vijayamohanan, Silver nanocluster redox-couple-promoted nonclassical electron transfer: an efficient electrochemical wolff rearrangement of α-diazoketones, Chem. - A Eur. J. 12 (2006) 859–864, https://doi.org/10.1002/chem.200500696.

[26] H. Nigar, G.S.J. Sturm, B. Garcia-Baños, F.L. Peñaranda-Foix, J.M. Catalá-Civera, R. Mallada, A. Stankiewicz, J. Santamaría, Numerical analysis of microwave heating cavity: combining electromagnetic energy, heat transfer and fluid dynamics for a NaY zeolite fixed-bed, Appl. Therm. Eng. 155 (2019) 226–238, https://doi.org/10.1016/j.applthermaleng.2019.03.117.

[27] L. Farzin, M. Shamsipur, L. Samandari, S. Sadjadi, S. Sheibani, Biosensing strategies based on organic-scaffolded metal nanoclusters for ultrasensitive detection of tumor markers, Talanta 214 (2020) 120886–120898, https://doi.org/10.1016/j.talanta.2020.120886.

[28] U. Kauscher, J. Penders, A. Nagelkerke, M.N. Holme, V. Nele, L. Massi, S. Gopal, T. E. Whittaker, M.M. Stevens, Gold nanocluster extracellular vesicle supraparticles: self-assembled nanostructures for three-dimensional uptake visualization, Langmuir 36 (2020) 3912–3923, https://doi.org/10.1021/acs.langmuir.9b03479.

[29] Y. Du, H. Sheng, D. Astruc, M. Zhu, Atomically precise noble metal nanoclusters as efficient catalysts: a bridge between structure and properties, Chem. Rev. 120 (2020) 526–622, https://doi.org/10.1021/acs.chemrev.8b00726.

[30] R. Jin, C. Zeng, M. Zhou, Y. Chen, Atomically precise colloidal metal nanoclusters and nanoparticles: fundamentals and opportunities, Chem. Rev. 116 (2016) 10346–10413, https://doi.org/10.1021/acs.chemrev.5b00703.

[31] R.L. Johnston, Atomic and Molecular Clusters, 1st ed., London, 2002. https://doi.org/10.1201/9780367805814.

[32] H. Qian, M. Zhu, Z. Wu, R. Jin, Quantum sized gold nanoclusters with atomic precision, Acc. Chem. Res. 45 (2012) 1470–1479, https://doi.org/10.1021/ar200331z.

[33] R.L. Johnston, The development of metallic behaviour in clusters, Philos. Trans. R. Soc. Lond. A. 356 (1998) 211–230, https://doi.org/10.1098/rsta.1998.0158.

[34] T. Tsukuda, H. Häkkinen. Protected Metal Clusters: From Fundamentals to Applications, first ed., Elsevier, 2015.

[35] Y. Piñeiro, J. Rivas, M.A. López-Quintela, The emergence of quantum confinement in atomic quantum clusters, in: Colloid. Foundantions Nanosci., Elsevier, 2014, pp. 81–105, https://doi.org/10.1016/B978-0-444-59541-6.00004-7.

[36] O.Krogh Andersen, Electronic structure of the fcc transition metals Ir, Rh, Pt, and Pd, Phys. Rev. B. 2 (1970) 883–906, https://doi.org/10.1103/PhysRevB.2.883.

[37] S. Roth, D. Carroll, Foundations of Solid State Physics: Dimensionality and Simmetry, 2019. https://doi.org/10.1002/9783527816590.

[38] H. Huang, H. du Toit, M.O. Besenhard, S. Ben-Jaber, P. Dobson, I. Parkin, A. Gavriilidis, Continuous flow synthesis of ultrasmall gold nanoparticles in a microreactor using trisodium citrate and their SERS performance, Chem. Eng. Sci. 189 (2018) 422–430, https://doi.org/10.1016/j.ces.2018.06.050.

[39] S. Biswas, J.T. Miller, Y. Li, K. Nandakumar, C.S.S.R. Kumar, Developing a millifluidic platform for the synthesis of ultrasmall nanoclusters: Ultrasmall copper nanoclusters as a case study, Small 8 (2012) 688–698, https://doi.org/10.1002/smll.201102100.

[40] K. Shimizu, Y. Miyamoto, A. Satsuma, Size- and support-dependent silver cluster catalysis for chemoselective hydrogenation of nitroaromatics, J. Catal. 270 (2010) 86–94, https://doi.org/10.1016/j.jcat.2009.12.009.

[41] F. Regali, L.F. Liotta, A.M. Venezia, V. Montes, M. Boutonnet, S. Järås, Effect of metal loading on activity, selectivity and deactivation behavior of Pd/silica-alumina catalysts in the hydroconversion of n-hexadecane, Catal. Today 223 (2014) 87–96, https://doi.org/10.1016/j.cattod.2013.08.028.

[42] N. Wang, Q. Sun, J. Yu, Ultrasmall metal nanoparticles confined within crystalline nanoporous materials: a fascinating class of nanocatalysts, Adv. Mater. 31 (2018) 1803966–2803989, https://doi.org/10.1002/adma.201803966.

[43] F. Morales-Lara, V.K. Abdelkader-Fernández, M. Melguizo, A. Turco, E. Mazzotta, M. Domingo-García, F.J. López-Garzón, M. Pérez-Mendoza, Ultra-small metal nanoparticles supported on carbon nanotubes through surface chelation and hydrogen plasma reduction for methanol electro-oxidation, J. Mater. Chem. A. 7 (2019) 24502–24514, https://doi.org/10.1039/c9ta08424j.

[44] G. Martinez, A. Malumbres, A. Lopez, R. Mallada, J.L. Hueso, J. Santamaria, Laser-assisted production of carbon-encapsulated Pt-Co alloy nanoparticles for preferential oxidation of carbon monoxide, Front. Chem. 6 (2018), https://doi.org/10.3389/fchem.2018.00487.

[45] L. Usón, V. Sebastian, A. Mayoral, J.L. Hueso, A. Eguizabal, M. Arruebo, J. Santamaria, Spontaneous formation of Au-Pt alloyed nanoparticles using pure nano-counterparts as starters: a ligand and size dependent process, Nanoscale 7 (2015), https://doi.org/10.1039/c5nr01819f.

[46] J. Strachan, C. Barnett, A.F. Masters, T. Maschmeyer, 4-Nitrophenol reduction: probing the putative mechanism of the model reaction, ACS Catal. 10 (2020) 5516–5521, https://doi.org/10.1021/acscatal.0c00725.

[47] K. Muthu, S. Priya, Green synthesis, characterization and catalytic activity of silver nanoparticles using Cassia auriculata flower extract separated fraction, Spectrochim. Acta - Part A Mol. Biomol. Spectrosc. 179 (2017) 66–72, https://doi.org/10.1016/j.saa.2017.02.024.

[48] A. Larrea, A. Eguizabal, V. Sebastián, Gas-directed production of noble metal-magnetic heteronanostructures in continuous fashion: application in catalysis, ACS

Appl. Mater. Interfaces 11 (2019) 43520–43532, https://doi.org/10.1021/acsami.9b15982.
[49] F. Yang, B. Wang, H. Su, S. Zhou, Y. Kong, Facilely self-reduced generation of Ag nanowires in the confined reductive siliceous nanopores and its catalytic reduction property, J. Alloy. Compd. 719 (2017) 30–41, https://doi.org/10.1016/j.jallcom.2017.05.160.
[50] B. Naik, S. Hazra, V.S. Prasad, N.N. Ghosh, Synthesis of Ag nanoparticles within the pores of SBA-15: An efficient catalyst for reduction of 4-nitrophenol, Catal. Commun. 12 (2011) 1104–1108, https://doi.org/10.1016/j.catcom.2011.03.028.
[51] H. Huo, Y. Jiang, T. Zhao, Z. Wang, Y. Hu, X. Xu, K. Lin, Quantitatively loaded ultra-small Ag nanoparticles on molecularly imprinted mesoporous silica for highly efficient catalytic reduction process, J. Mater. Sci. 55 (2020) 1475–1488, https://doi.org/10.1007/s10853-019-04054-x.
[52] B. Baruah, G.J. Gabriel, M.J. Akbashev, M.E. Booher, Facile synthesis of silver nanoparticles stabilized by cationic polynorbornenes and their catalytic activity in 4-nitrophenol reduction, Langmuir 29 (2013) 4225–4234, https://doi.org/10.1021/la305068p.
[53] X. Cheng, D. Wang, J. Liu, X. Kang, H. Yan, A. Wu, Y. Gu, C. Tian, H. Fu, Ultra-small Mo2N on SBA-15 as a highly efficient promoter of low-loading Pd for catalytic hydrogenation, Nanoscale 10 (2018) 22348–22356, https://doi.org/10.1039/c8nr06916f.
[54] R. Knorr, Alkylidenecarbenes, alkylidenecarbenoids, and competing species: which is responsible for vinylic nucleophilic substitution, [1 + 2] cycloadditions, 1,5-CH insertions, and the Fritsch−Buttenberg−Wiechell Rearrangement? Chem. Rev. 104 (2004) 3795–3850, https://doi.org/10.1021/cr030616h.
[55] A. Fürstner, P.W. Davies, Catalytic carbophilic activation: catalysis by platinum and gold πacids, Angew. Chem. Int. Ed. 46 (2007) 3410–3449, https://doi.org/10.1002/anie.200604335.
[56] P. Sivaguru, S. Cao, K.R. Babu, X. Bi, Silver-catalyzed activation of terminal alkynes for synthesizing nitrogen-containing molecules, Acc. Chem. Res. 53 (2020) 662–675, https://doi.org/10.1021/acs.accounts.9b00623.
[57] O.P. Pereshivko, V.A. Peshkov, J. Jacobs, L. Van Meervelt, E.V. Van der Eycken, Cationic gold- and silver-catalyzed cycloisomerizations of propargylic ureas: a selective entry to oxazolidin-2–imines and imidazolidin-2–ones, Adv. Synth. Catal. 355 (2013) 781–789, https://doi.org/10.1002/adsc.201200905.
[58] H. Feng, D.S. Ermolat'ev, G. Song, E.V. Van der Eycken, Synthesis of oxazolidin-2–ones via a copper(I)-catalyzed tandem decarboxylative/carboxylative cyclization of a propiolic acid, a primary amine and an aldehyde, Adv. Synth. Catal. 354 (2012) 505–509, https://doi.org/10.1002/adsc.201100608.
[59] C. Villiers, J. Dognon, R. Pollet, P. Thuéry, M. Ephritikhine, An isolated CO_2 adduct of a nitrogen base: crystal and electronic structures, Angew. Chem. - Int. Ed. 49 (2010) 3465–3468, https://doi.org/10.1002/anie.201001035.
[60] M. Yoshida, T. Mizuguchi, K. Shishido, Synthesis of oxazolidinones by efficient fixation of atmospheric CO 2 with propargylic amines by using a silver/1,8-diazabicyclo[5.4.0] undec-7-ene (DBU) dual-catalyst system, Chem. Eur. J. 18 (2012) 15578–15581, https://doi.org/10.1002/chem.201203366.
[61] S.S. Islam, S. Biswas, R. Ali Molla, N. Yasmin, S.M. Islam, Green synthesized AgNPs embedded in COF: an efficient catalyst for the synthesis of 2-oxazolidinones and α-alkylidene cyclic carbonates via CO_2 fixation, ChemNanoMat 6 (2020) 1386–1397, https://doi.org/10.1002/cnma.202000284.
[62] S. Ghosh, S. Riyajuddin, S. Sarkar, K. Ghosh, S.M. Islam, Pd NPs decorated on POPs as recyclable catalysts for the synthesis of 2-oxazolidinones from propargylic amines via atmospheric cyclizative CO_2 incorporation, ChemNanoMat 6 (2020) 160–172, https://doi.org/10.1002/cnma.201900505.
[63] R. Khatun, S. Biswas, I.H. Biswas, S. Riyajuddin, N. Haque, K. Ghosh, S.M. Islam, Cu-NPs@COF: A potential heterogeneous catalyst for CO2fixation to produce 2-oxazolidinones as well as benzimidazoles under moderate reaction conditions, J. CO_2 Util. 40 (2020) 101180–101191, https://doi.org/10.1016/j.jcou.2020.101180.